Article

Low Temperature Effect on the Mechanical Properties of EH36 with Strain Rates

Jing Zhang [1], Xuelei Kang [1], Xinghua Shi [1,2,*], C. Guedes Soares [2] and Ming Song [1]

[1] School of Naval Architecture and Ocean Engineering, Jiangsu University of Science and Technology, Zhenjiang 212100, China
[2] Centre for Marine Technology and Ocean Engineering (CENTEC), Instituto Superior Técnico, Universidade de Lisboa, 1049-001 Lisbon, Portugal
* Correspondence: xinghuashi@just.edu.cn; Tel.: +86-15896380832; Fax: +86-51184404433

Abstract: With the expansion of the Arctic route, the safety of ship crossing the area in light of the low temperature and ice has become of focus, especially with regards to the ship's structure. The mechanical properties of the material making up the ship's structure may not be suitable for the Arctic environment. A series of quasi-static and dynamic tests were performed to investigate the behaviour of EH36 steel, which is used to build Arctic ships, at temperatures ranging from 20 °C to −60 °C. The yield and ultimate tensile stress increased more than 10% as the temperature decreased from 20 °C to −60 °C, whereas the toughness decreased as the temperature decreased. A formula was derived to illustrate the relationship between the temperature reduction and the yield strength by fitting the experimental data. Four common constitutive rigid-perfectly plastic, elastic-perfectly plastic, bilinear elastic-plastic, and multi-linear elastic plastic models were fitted to simulate the hull structure under static loading and low temperature. Additionally, the strain rate effect of EH36 steel at low temperatures was illustrated by quasi-static and high-speed impact tests. A constitutive model including the low temperature and strain rate was introduced based on a modified Cowper-Symonds model, in which the coefficients of the constitutive model are fitted by the test results. It is improved by an iterative numerical method used to obtain more accurate coefficients using a series of numerical analyses. Detailed finite element simulations of the experiment conditions revealed that the constitutive model accurately predicts the dynamic response at low temperatures.

Keywords: constitutive model; low temperature; cowper-symonds; strain rate; dynamic behaviour

1. Introduction

As the air temperature has been increasing over the last several years, the Arctic shipping routes are becoming suitable for shipping for more than 4 months per year. This route reduces shipping costs significantly, especially from China to USA and Europe. However, shipping in the Arctic is a challenge for common ships, due to the threats related to low temperatures and collision with floating ice. The design and manufacture of Arctic ships are becoming an increasingly interesting topic. Some rules or guidelines were introduced for Arctic ships by the Classification Societies or other organizations [1–3]. However, the interaction mechanics of ships and ice is not fully understood, including the constitutive properties of steel at low temperature, and of the ice. While ships are crossing the ice area, repeated impacts of ice on the hull will occur, and proper methods to account for them need to be available [4]. As the basic input of the ship–ice interaction response, the constitutive relationship is one of the important factors that needs to be studied. The dynamic load and the low temperature may affect the ship's structure simultaneously. Strain rate will have a significant effect on the collision or impact response of steel or similar material with the characteristics of strain rate sensitivity [5]. It is necessary to discuss the dynamic mechanics of the ship structure's steel at low temperatures based on the quasi-static mechanical properties. A series of quasi-static and dynamic material tests

should be performed. However, some special materals, such as mild steel and high-tensile steel, have been studied at low teperatures, except for EH36, which is used to build the Arctic ships, and no common constitutive model has been presented.

As the temperature is decreasing, the yield tensile stress will increase for steel, but the toughness will reduce. If the ship structure is subjected to the impact of ice, it is necessary to predict the response accurately, including the strain rate's effect on the ship's steel. The increased crashworthiness was studied in arctic conditions at sub-zero temperatures by Ehlers [6]. The steel material characteristics obtained by the quasi-static tensile material standard tests were used to perform the comparative collision simulations. A test database covering low temperatures up to −60 °C was given by Paik [7] from a series of static, quasi-static, and dynamic tests for mild steel, high-tensile steel (AH32, DH32 and DH36), aluminium alloy 5083-O, and stainless steel 304 L. Except for these tests, limited research was performed on the mechanics of the ship's steel at low temperatures. Low and middle strain rates were included in the tests by Choung et al. [8] at a low temperature (−40 °C), room temperature, and a high temperature (200 °C) to investigate the hardening behaviour. The EH series high-tensile steel is another material for Arctic ships recommended by DNV [9], ABS [2], and IACS [10], which will be studied in this paper.

Numerous researchers have published their experimental results on the effect of strain rate on the behaviour of structural steel and the mechanical properties of mild steel. The mechanical testing of metals at a high strain rate (10^2–10^4 s^{-1}) is typically performed with the Kolsky bar, also widely known as the Split Hopkinson Pressure Bar (SHPB) [11]. Low ($\dot{\varepsilon} - 10^{-3}$ s^{-1}), intermediate ($\dot{\varepsilon} - 1$ s^{-1}), and high ($\dot{\varepsilon} - 10^3$ s^{-1}) strain rate experiments are performed on dog-bone and notched specimens extracted from 1.4 mm thick TRIP780 steel sheets. Experiments in the intermediate range of strain rates ($\dot{\varepsilon} - 1{\sim}10$ s^{-1}) are typically carried out in servo-hydraulic testing machines, whereas high strain rate experiments (100–1000 s^{-1}) are usually performed in the Split Hokinson Bar system [12]. Various authors have studied the effect of strain rate at room temperature; both the behaviour of aluminium and steel have been studied, as the first is not strain-sensitive and the latter is [13]. Different constitutive models have been proposed to represent the behaviour of steel [5,14].

High temperatures induce strain ageing of the metal material. The high strain increases the strength but decreases the ductility combined with the high temperatures for the low-alloy structural carbon steel S335 [15]. The mechanical behaviour of a high strain rate that induced partially damaged mild steel under various temperature test conditions has been reported by Mirmomeni et al. [16]. High temperatures are the dominant factor, as the temperature is over 450 °C. Nemat-Nasser and Guo [17] predicted the compressive mechanical behaviour of this steel within a very large strain rate (from 0.001 to 10,000/s) and temperature ranges (−196.15 °C–726.85 °C) and only investigated −196.15 °C. The low temperature of −196 °C induces the transformation of the ductile-to-brittle behaviour of the stainless steel weldments including 304 L and 316 L, but there is little decrease in the impact energy [18]. Getter et al. [19] designed a novel high-rate testing apparatus to conduct uniaxial tensile tests of two marine types of steels under strain rates ranging from 13 to 250 s^{-1}. Chen, et al. [20] performed a series of quasi-static and dynamic uniaxial tensile tests within the range of 0.001–288 s^{-1} strain rates to study the rate-dependent mechanical properties of Q420 steel using the INSTRON and Zwick/Roell HTM5020 testing machine. Su et al. [21] tested the tensile mechanical behaviour of DH 36 steel. The strain rate range was from 0.001 to 3000/s, and the initial specimen temperatures were 19.85–526.85 °C. The flow mechanism combined with the strain rate of an Ni-based superalloy was investigated by Detrois et al. [22] under high temperatures more than 1000 °C using isothermal compression testing. Flow stress models were studied for different high temperatures.

Based on the available experimental results, some constitutive models considering the influence of strain, strain rate, and temperature on the strain-hardening behaviour have been proposed by several researchers. Forni et al. [23] developed the constitutive model

of S355 structural steel by using the Johnson–Cook (J-C) model and Cowper-Symonds (C-S) model [24]. Shi et al. [25] developed a revised multi-linear constitutive model of high-strength structural steel based on material property data of Q500, Q550, and Q690 steels (over 10,000 samples). The change in yield strength between high-strength structural steels inevitably led to differences in mechanical properties and dynamic behaviour. The experimental stress–strain data obtained from high strain rate compression tests using SHPB by Bobbili et al. [26] over a range of tempering temperatures (500–650 °C), strains (0.05–0.2), and strain rates (1000–5500 s^{-1}) were employed to formulate the J-C model to predict the high strain rate deformation behaviour of high-strength armour steels.

Many studies on the mechanical properties of steel consider the effects of strain rate and temperature. However, few studies focused on the behaviour of stress–strain curves at low temperatures and strain rates. The Cowper-Symonds representation of material strain rate sensitivity is commonly employed in finite element impact simulations of steel marine structures; Cowper-Symonds coefficients of $C = 40.4$ and $P = 5.00$ were employed for mild steel [27]. However, the Cowper-Symonds parameters vary widely among different studies of mild steel [28,29]. In this paper, the experiment aimed to investigate the complex behaviour of different strain rates induced by ship–ice collision at low temperatures. The material mechanical properties from low to high strain ranging from 2×10^{-4} to 2000 s^{-1} were obtained from quasi-static tests by material testing machine (MTS) and dynamic material tests using the split Hopkinson pressure bar (SHPB) for EH36. A constitutive model was presented with low temperature and strain rate by the test and numerical data. The stress–strain curves provide a reliable material behaviour, covering strain rates ranging from 2×10^{-4} to 2000 s^{-1} and temperatures from 20 °C to −60 °C.

2. Experimental Program

2.1. Test Specimen

No rules or guidelines for the test specimen at low temperatures have yet been published now. Paik [7] performed the tension test at low temperatures, according to the standard of the tension testing of metallic materials by ASTM [30]. However, the test methods in the standard only cover the testing of metallic materials at room temperature (10–38 °C). Low temperatures increase the yield strength of the steel during the quasi-static tension process. The same specimen may be used at low temperatures.

A specimen was designed for the quasi-static test at low temperatures, as shown in Figure 1a. The sheet-type standard specimen was of 6 mm thickness, 12.5 mm width in the middle, and 20 mm width in the grip section. The length of the grip section was 50 mm. The test was performed in a low-temperature box, with one end fixed by wedge grips and the other by a pin. It was a bone type with a wider end compared with the standard specimen at normal temperature. There was a hole with a diameter of 10 mm on the centre line in the wider end to connect the specimen end test set-up, as shown in Figure 2c. A bar with a bolt through the hole in the specimen was used to connect the specimen to the upper loading equipment. The wider end was three times wider than the other end to eliminate the cross-section reduction effect. It was also confirmed that the failure happens in the middle of the specimen, as shown in Figure 3.

The length of the dynamic specimen was 3 mm and the diameter was 6 mm. The surfaces of the specimen were polished to ensure their smoothness. There were no residual stress and machining defects in the specimen.
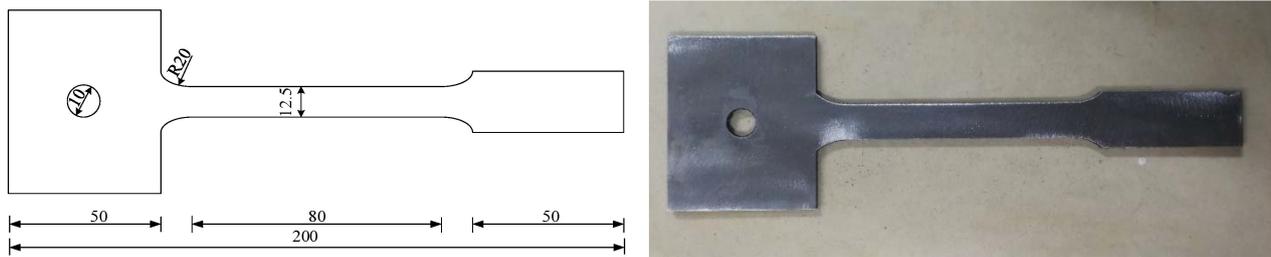
(**a**) Quasi-static test specimen.
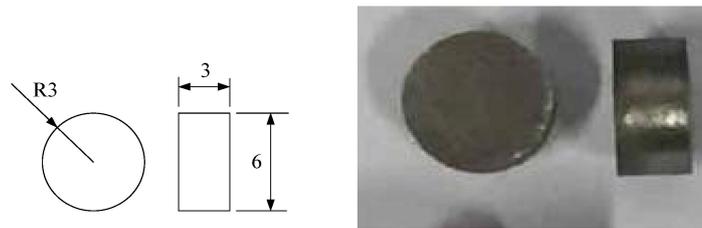
(**b**) Dynamic test specimen.

Figure 1. Geometry test specimen (unit: mm).
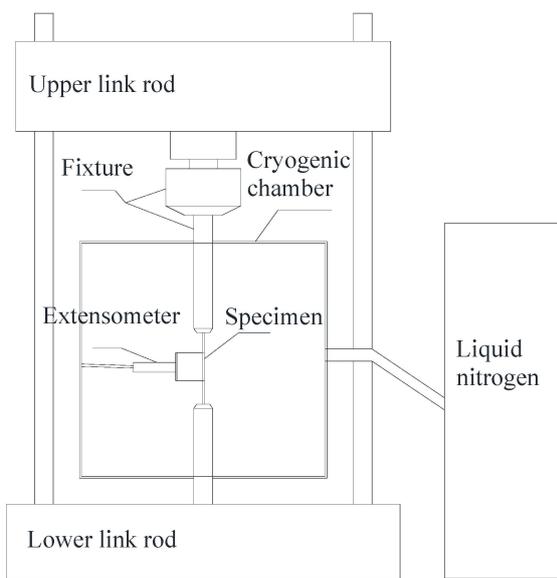
(**a**) Schematic of the quasi-static tensile experiment.   (**b**) Experimental setup for low strain rate tensile tests.

Figure 2. *Cont*.
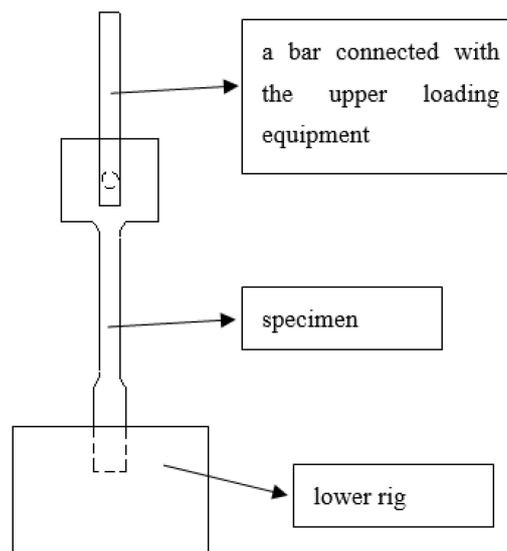
(**c**) Details of the specimen connection.

Figure 2. Quasi-static test setup at low temperatures.

Figure 3. Failure of the quasi-static test specimen.

2.2. Test Setup

2.2.1. Quasi-Static and Low Velocity Tests

The quasi-static tension tests were performed by Material Testing Systems (MTS 810) with a maximum loading capacity of 500 KN, as the specimen was in a cryogenic chamber designed for keeping a low-temperature environment using liquid nitrogen. The arrangement of the test setup is shown in Figure 2a,b. Two holes were opened on the top and bottom surface of the chamber to install the specimen; the bottom end gripped and the top end pinned, as shown in Figure 2c. An extensometer for the temperate range of −80 to 80 °C was set on the surface of the specimen to measure the strain. The test section had to be completely immersed in the constant low-temperature chamber.

The design strain rate of quasi-static tension tests is $2 \times 10^{-4}\,\mathrm{s}^{-1}$. Some low velocity tension experiments at the strain rates of 0.01, 0.1 and 1 s^{-1} were also performed by the MTS in Figure 2. The axial tension tests of two specimens were carried out at ambient temperature (room temperature, 20 °C, or low temperature). The specimen was fixed in the temperature chamber for more than 1 h until the temperature of the specimen achieved the

target value. During the process, the shrinking had to be monitored by the extensometer during the cooling process. If the deformation happened as the strain, the loading bar needed to be adjusted for the MTS.

2.2.2. Dynamic Test

The experimental data of high strain rates were obtained from high-velocity impact tests using Split Hopkinson Pressure Bar (SHPB) in the Explosions and Shock Lab of Nanjing University of Science and Technology, covering a wide range of strain rates 100–2000 s^{-1}. Several high strain rate tests were performed by SHPB at room temperature and low temperatures.

The entire SHPB setup consisted of several pieces of equipment, as shown in Figure 4. Compared to the traditional equipment, a low temperature box was added only with a hole in the side of the input bar. The size of the hole was a little bigger than the input bar to ensure the impact process. The low temperature was provided by the input of ammonia.

(**a**) Experimental setup for high strain rate compressive tests
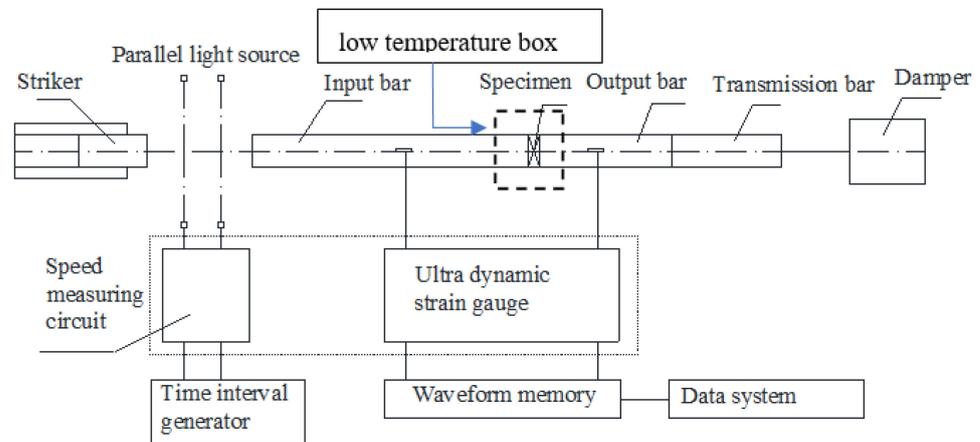
(**b**) Schematic of SHPB setup for steel testing.

Figure 4. Setup of Split Hopkinson Pressure Bar (SHPB) test system.

An SHPB system has two pressure bars, an input or incident bar, and another called output or transmitted bar, as shown in Figure 4b [31]. The yield strength of the pressure bar determines the maximum stress attainable within the deforming specimen because the cross-section of the specimen approaches that of the pressure bar during deformation. A rectangular compression wave of well-defined amplitude and length is generated in the input bar when the striker bar impacts it. As this wave reaches the specimen, part of the pressure wave is transmitted into the specimen and output bar, and part is reflected to the incident bar.

The Input wave, reflection wave, and transmission wave are measured by the ultra-dynamic strain gauge. Based on the one-dimensional and uniform assumption, the average

dynamic stress, strain, and strain rate of the tested specimen are determined under a one-dimensional stress state:

$$\sigma(t) = \frac{A}{2A_s}E(\varepsilon_i + \varepsilon_r + \varepsilon_t) = E\frac{A}{A_s}\varepsilon_t \qquad (1)$$

$$\varepsilon(t) = \frac{C_e}{l_0}\int_0^t (\varepsilon_i - \varepsilon_r - \varepsilon_t)dt = -\frac{2C_e}{l_0}\int_0^t \varepsilon_r dt \qquad (2)$$

$$\dot{\varepsilon}(t) = \frac{C_e}{l_0}(\varepsilon_i - \varepsilon_r - \varepsilon_t) = -\frac{2C_e}{l_0}\varepsilon_r \qquad (3)$$

where ε_i, ε_r, and ε_t are the strains of the input wave, reflection wave, and transmission wave, respectively. σ is the stress; ε is the strain; $\dot{\varepsilon}$ is the strain rate; E is the elastic modulus of the pressure bar; C_e is the elastic wave velocity; A is the cross-section area of the pressure bar; and l_0 and A_s are the initial length and initial cross-section of the specimen, respectively.

3. Quasi-Static Response

3.1. Test Results

A series of quasi-static tests on EH36 steel was performed by the MTS system combined with the low-temperature chamber at a strain rate of $2 \times 10^{-4}\,\text{s}^{-1}$. The test temperatures ranged from room temperature (20 °C) to low temperatures (0 °C, −20 °C, −40 °C, and −60 °C). The engineering and true stress–strain curves of the EH36 steel at low temperatures are shown in Figure 5. Low temperature will increase the yield strength of EH36. The average tested yield strength and ultimate tensile strength at different temperatures are shown in Figure 6, where σ_s is the yield stress and σ_u is the ultimate tensile stress. As the temperature decreased from 20 °C to −60 °C, the yield strength was increased by 11.6%, and the ultimate tensile strength was 11.3%. The nonlinearly increase trend lines were fitted by quadratic polynomial.

(**a**) Engineering stress–strain curves   (**b**) True stress–strain curves
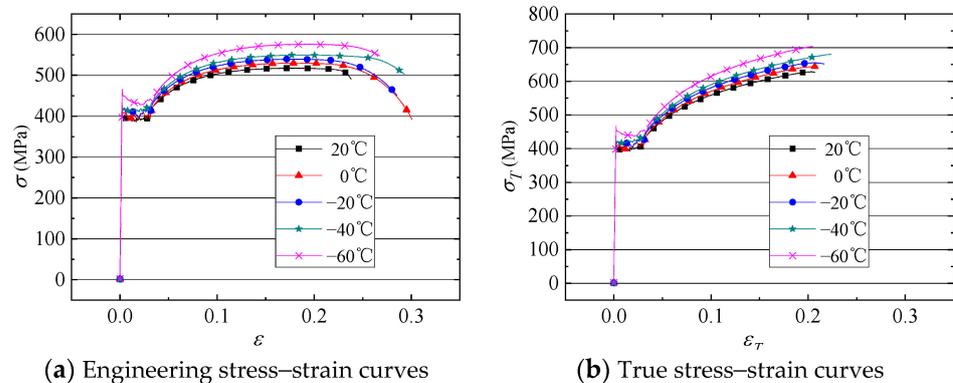
Figure 5. Stress–strain curves of EH36 at different temperatures.

The yield stress of steel can be approximated from the experimental data shown in Figure 6a as follows:

$$\sigma'_s = f_{(T'-T)}\sigma_s \qquad (4)$$

where T is room temperature (20 °C), T' is the target temperature, σ'_S is the quasi-static yield stress of EH36 steel at temperature T', and $f_{(T'-T)}$ is a formula that indicates the relationship obtained from EH36 steel quasi-static tensile test at different low temperatures. Based on the fitted curve in Figure 6a, the relationship formula can be a quadratic function related to the temperature difference $(T' - T)$, $f_{(T'-T)} = a(T' - T)^2 + b(T' - T) + c$. a, b, c are the empirical coefficients and σ_s is the yield stress of quasi-static at room temperature. $a = 1.303 \times 10^{-5}$, $b = -3.071 \times 10^{-4}$, $c = 1.004$.

(a) Yield stress

(b) Ultimate tension stress
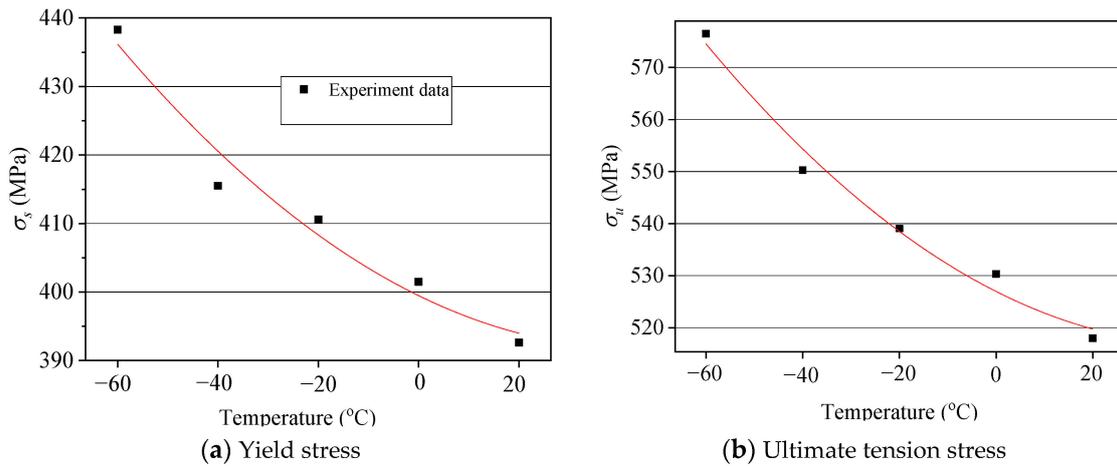
Figure 6. Yield stress and ultimate tension stress at different temperatures (average).

Except for the yielding and ultimate tensile stress, low temperatures affects the engineering fracture strain significantly, as shown in Figure 7. The low temperatures induce a decrease in the engineering fracture strain, as well as the strain rate. Under the same temperature, the engineering fracture strain decreases with the increase in the strain rate.

(a) 0 °C

(b) −20 °C

(c) −40 °C

(d) −60 °C
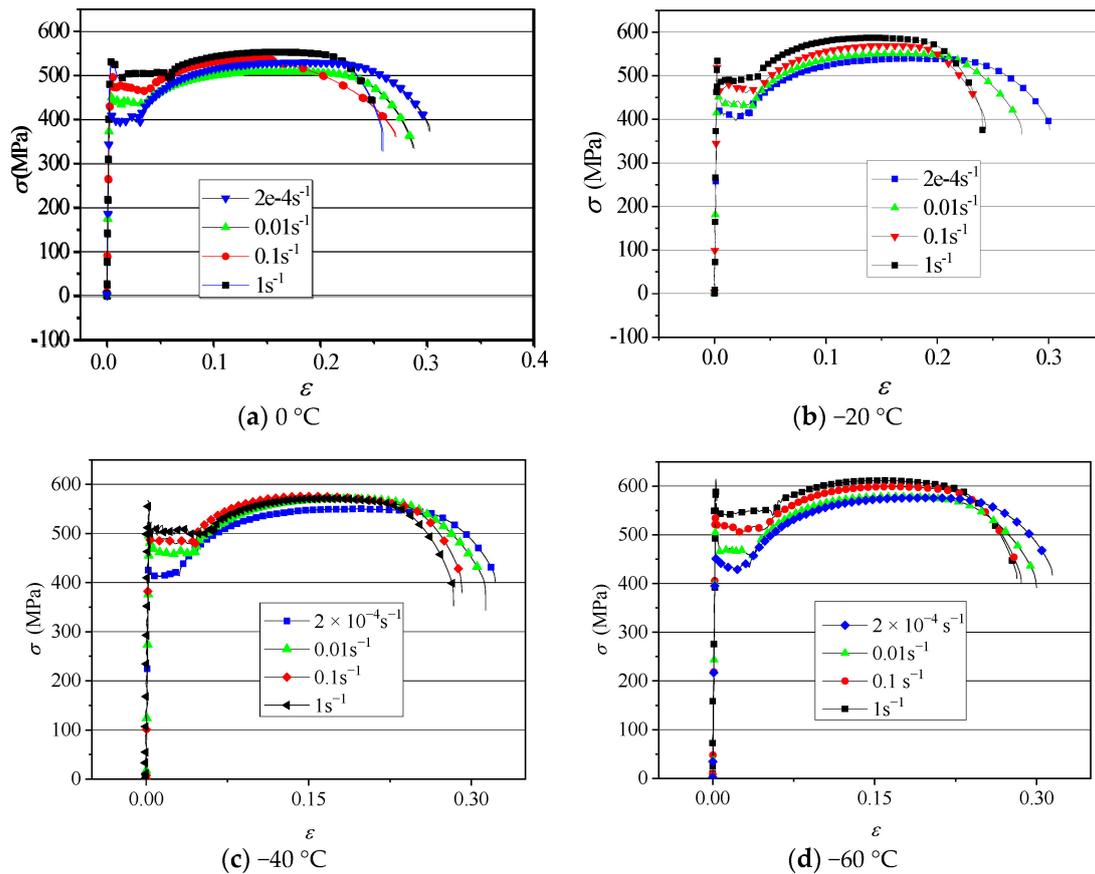
Figure 7. Stress–strain curves of EH36 at low strain rates from −60 °C to 0 °C.

3.2. Simplified Quasi-Static Constitutive Relationship

The interaction mechanics of ice and ships or offshore structures will show strong nonlinearity, as the plastic and larger deformation will happen in the loading process for the ship's steel material. It is suitable to strengthen the structure by adding more stiffeners or increasing the plate thickness to avoid plastic deformation, according to the traditional

design method. However, a flexible way involves limited plastic deformation, which can lighten the ship's structure within the design of Arctic ships, in accordance with the Rules [2]. The elastic constitutive model using linear Hooke's relationship is not suitable for the study of structural mechanics in the Arctic environment. It is necessary to study the plastic constitutive models as the input for the structural analysis.

The quasi-static constitutive relationship is discussed firstly based on the engineering stress–strain curves, according to the quasi-static test results of the EH36 steel. As shown in Figure 8, the real stress–strain curve consists of three stages: linear elastic part determined by elastic modulus E, yielding, and the hardening part. It is nonlinear and too complicated to carry out the plastic analysis. Considering the assumptions and simplifications given by the analysis objective, four constitutive models were derived as follows:
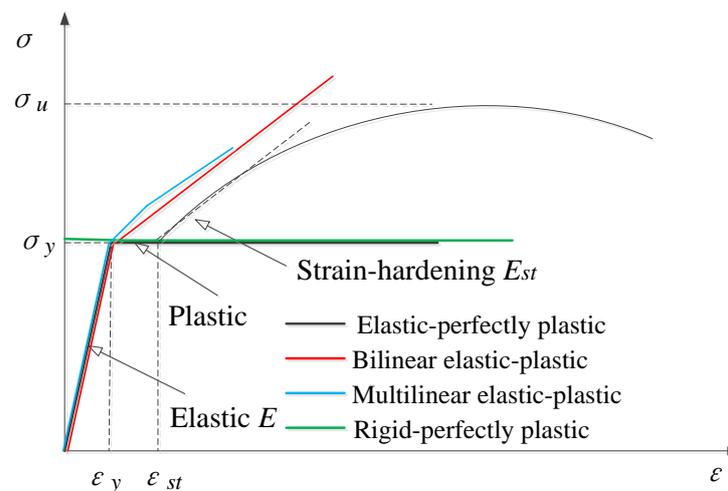
Figure 8. Quasi-static stress–strain relationship models.

(1) Elastic-perfectly plastic: as the stress reaches yield one, the material will be at the plastic stage. The yielding flow is considered, neglecting the hardening effect, when the strain is smaller than the yield strain, Hooke's Law is used to describe the linear relationship with the elastic modulus. As the strain reaches the yield strain, the stress becomes constant and equal to the yield stress, as illustrated by the black line shown in Figure 8.

(2) Bilinear elastic-plastic: the hardening effect is included but neglects the flow stress. The first relationship is linear elastic. As the stress reaches yield stress, a second linear relationship is used to describe the stress–strain curve determined by the tangent modulus E_{st}. It is shown in Figure 8 by the red line.

(3) Multi-linear elastic-plastic: an extended model of bilinear elastic hardening constitutive model. The hardening curve is defined by a multi-linear function, as shown in Figure 8 by the blue line.

(4) Rigid perfectly plastic: a simplified model of the elastic-perfectly plastic constitutive model. Elastic strain is neglected, without the plastic hardening. As the stress reaches the yielding value, the plastic flow happens.

Due to the simplification, models (1) and (4) were used to study the ultimate strength or plastic deformation analysis of structures. Models (2) and (3) were used to study the elastic and plastic response of the structure.

As the tensile stress was close to the ultimate strength, a fracture occurred in the middle part of the test section. The necking phenomenon was observed. The stress–strain curve of EH36 steel at room temperature is shown in Figure 9 as per the test. The result is a yield stress of 392.6 MPa and an ultimate tensile stress of 516.8 MPa.
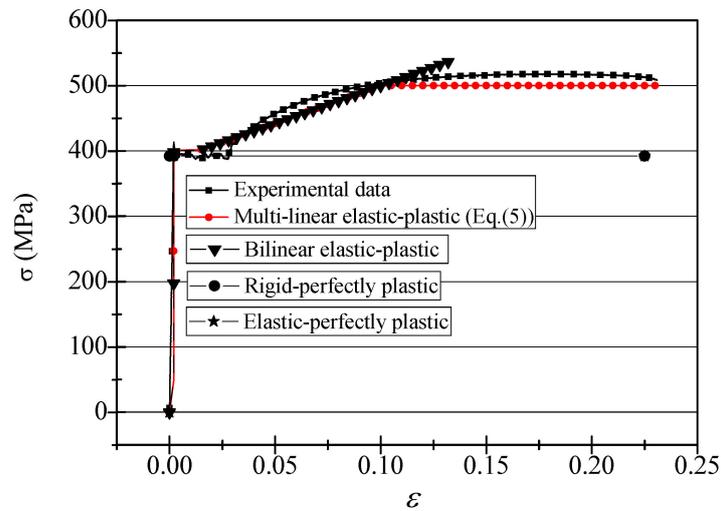
Figure 9. Fitted constitutive models of EH36 steel at room temperature.

The four constitutive models shown in Figure 8 are fitted according to the experiment data, and the multi-linear elastic-plastic relationship is fitted as follows:

$$
\begin{aligned}
\sigma &= 2.07 \times 10^5 \cdot \varepsilon & (\varepsilon \leqslant 0.002) \\
\sigma &= 1154 \cdot \varepsilon + 392.6 & (0.002 < \varepsilon \leq 0.1) \\
\sigma &= 500 & (\varepsilon > 0.1)
\end{aligned}
\tag{5}
$$

Figure 9 shows the fitting of the constitutive model curves and stress–strain experimental data at room temperature. The constitutive relationship can be derived based on the yield stress determined by Equation (4).

4. Dynamic Constitutive Model by Numerical Results

4.1. Test Results

A series of dynamic tests were performed at low temperatures including low strain rates 0.01, 0.1, and 1 s^{-1} and high strain rates ranging from 700 to 1800 s^{-1}. Dynamic stress–strain curves of EH36 steel at low strain rates were obtained using MTS at room temperature, as illustrated in Figure 10a. High strain rate tests were performed by SHPB. The stress, strain, and strain rate were calculated using Equations (1)–(3) described in Section 2.2. Figure 10b shows the stress–strain curves with varied high strain rates of 769, 932, 1030, 1312, and 1685 s^{-1} at room temperature.

(a) MTS test

(b) SHPB test
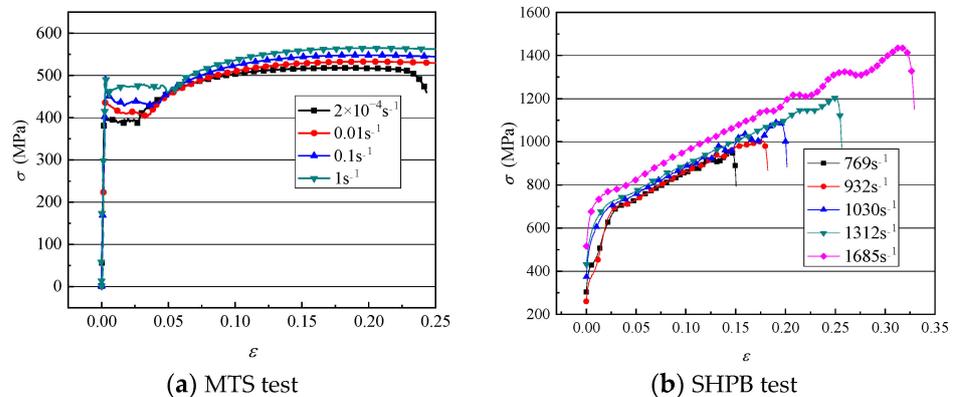
Figure 10. Stress–strain curves of EH36 at different strain rates, room temperature.

Table 1 lists the yield stress of EH36 steel from low to high strain rates. Figure 11 shows the variation of yield stress with strain rate; the experimental data were fitted by

quadratic polynomial. It can be observed that the yield stress of steel increases as the strain rate increases, from 417.6 MPa at 0.01 s^{-1} to 736.26 MPa at 1685 s^{-1}. Compared with the quasi-static results, the yield stress increased by 6.4% with a strain rate of 0.01 s^{-1} and 87.5% with 1685 s^{-1}. The strain rate dependency characteristics of the test material at room temperature are indicated.

Table 1. Dynamic mechanical properties of EH36 steel at room temperature.

Strain rate/s^{-1}	0.01	0.1	1	769	932	1030	1312	1685
Yield stress/MPa	417.6	434.52	443.24	641.65	659.46	676.53	698.23	736.26
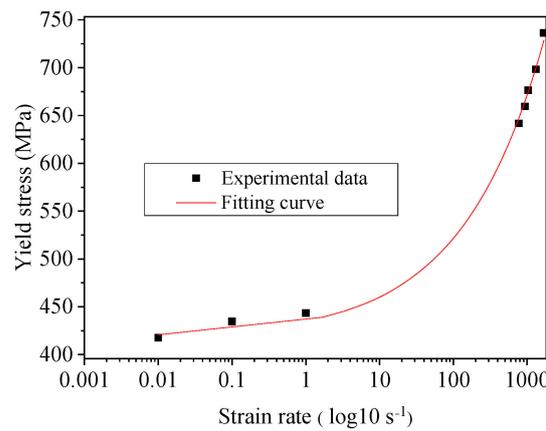
Figure 11. Variation of yield stress with strain rate.

The stress–strain curves of steel over a range of strain rates on the order of 0.01 to 1 s^{-1} from −60 °C to 0 °C are shown in Figure 7. High stain rate stress–strain curves over a range of strain rates on the order of 700 to 1900 s^{-1} from −40 °C to 0 °C are shown in Figure 12.
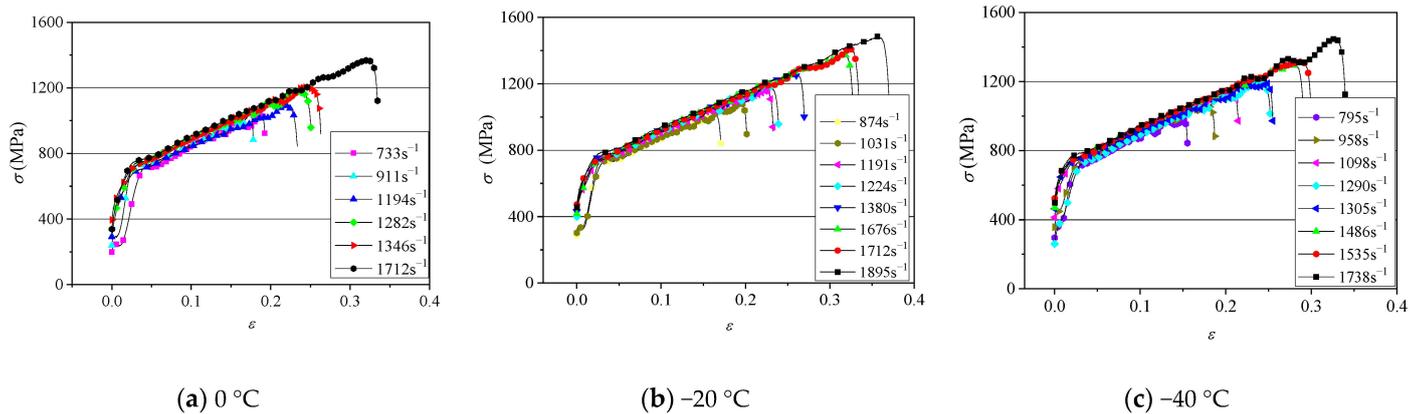
Figure 12. Stress–strain curves of EH36 at high strain rate from −40 °C to 0 °C.

The temperature effect on the stress–strain curves is illustrated in Figure 13. The yield stresses increase as the temperature decreases. However, the increasing trend of the yield stress becomes slow at low temperatures compared with yield stress at room temperature, especially at the high strain rate of more than 1200 s^{-1}, as shown by the dash lines in Figure 13b.
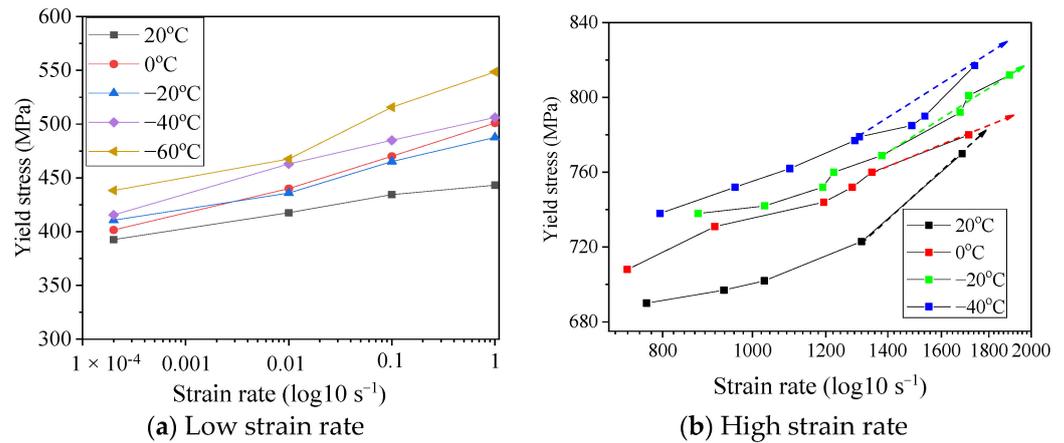
Figure 13. Yield stress at different temperatures.

4.2. Dynamic Constitutive Relationship with Strain Rate Effect and Low Temperature

The low temperature and the strain rate increases the yield stress. However, now there is no comprehensive constitutive model to describe the stress–strain relationship with the strain rate and low-temperature effect. To predict the response to the ship–ice interaction accurately, a dynamic constitutive model depending on the strain rate and low temperature may be presented as:

$$\sigma = f(\varepsilon, \dot{\varepsilon}, T) \tag{6}$$

It is difficult to establish a constitutive model combining the strain rate and low temperature directly. A function that decouples the combined effect may be written as:

$$\sigma = f_1(\varepsilon, \dot{\varepsilon}) \times f_2(\varepsilon, T) \tag{7}$$

There are several constitutive models to describe the strain rate sensitivity material. Almost all the models presented are based on experimental data. The Cowper-Symonds (CS) model is generally adopted to simulate the relationship with strain rate effect. It is written in the following form:

$$\frac{\sigma_{yd}}{\sigma_s} = 1 + \left(\frac{\dot{\varepsilon}}{C}\right)^{1/P} \tag{8}$$

where σ_{yd} is the dynamic yield stress, and C and P are material constants.

Combining the quasi-static constitutive model with the low-temperature effect, the dynamic stress depicting the effect of the strain rate and the low temperature has been expressed based on the Cowper-Symonds model. It is written as follows:

$$\sigma_{yd} = \left[1 + \left(\frac{\dot{\varepsilon}}{C}\right)^{\frac{1}{P}}\right]\left[f_{(T'-T)}\sigma_s\right] \tag{9}$$

where $f_{(T'-T)}$ is the empirical formula of the low-temperature effect, described in Equation (4), where σ_s is the yield stress of steel at room temperature.

According to the experimental results of yield stress–strain rate at room temperature in Figure 11, Equation (9) is fitted by the test data. The constitutive parameters C and P are 2370.6 and 4.00, respectively.

The constants of C and P at different low temperatures are fitted by the test data including low strain rate and high strain rate in the case of 20 °C, 0 °C, −20 °C, and −40 °C and low strain rate in the case of −60 °C, as listed in Table 2. Due to the limited sample, the values C and P fluctuate in a small range, except for −60 °C including only a low strain rate.

Table 2. *C* and *p* values at different temperatures.

Temperature	20 °C	0 °C	−20 °C	−40 °C	−60 °C
C	2370.6	2639.4	2453.6	2619.5	225.42
P	4.00	5.40	4.60	4.20	3.95

The constitutive model described in Equation (9) is the basic input of the ship–ice interaction analysis in icy waters. A series of numerical analyses was performed to validate the accuracy of the constitutive relationship under the test load conditions.

4.3. Improved Model

The constant values of the *C* and *P* in Equation (9) are fitted by the test results at a certain temperature, as shown in Table 2. However, only some samples are given for each temperature. The parameters may be not accurate enough as a result of the limited samples, especially when the combined effect of strain rate and low temperature is included.

An iterative approximate method was introduced to achieve the target value based on the test and numerical results, as shown in Figure 14. The steps are as follows:
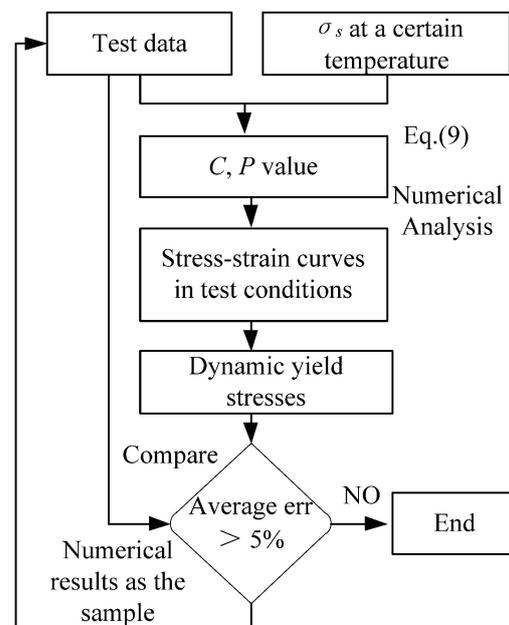
Figure 14. Flowchart of the iterative approximated method.

(1) Using the test data and the quasi-static yield stress at a certain temperature, the values of *C* and *P* in Equation (9) are fitted by the least square method.

(2) The *C*, *P* and the constitutive relationship in Equation (9) are the input to a series of numerical analyses of test conditions.

(3) The dynamic yield stress obtained by numerical analysis is compared with the one from tests. If the average error is smaller than 5%, the fitted values are accepted.

(4) If the error between the yield stress by numerical analysis and tests is large, with an average error larger than 5%, the numerical results are treated as the sample to refit the *C*, *p* values.

(5) Using the new *C*, *p* values, perform steps (2)–(4).

4.4. Numerical Models

The FE model of the MTS specimen is shown in Figure 15. The SHPB tests are simulated numerically by ABAQUS. The S4R element is employed in the numerical model with a mesh size of 2 mm and refined mesh in the middle area. The load is applied on one

end of the specimen at a certain velocity, and the other end is fully clamped. The model defined by Equation (9) in ABAQUS was adopted as the constitutive model of EH36 steel.
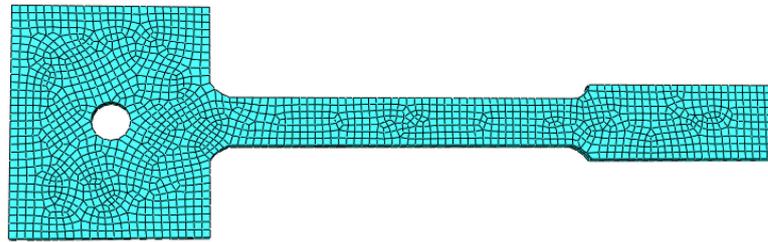
Figure 15. FE model of MTS specimen.

Figure 16 gives the FE model, simulated using solid elements C3D with a mesh size of 2 mm. The mesh size convergence was studied using a series of numerical analyses of the mild steel in [27]. The elastic modulus of the specimen was 2.07E5 MPa and Poisson ratio was 0.3. The impact bar, input bar, and output bar were also simulated by the solid element. The elastic modulus was 210 GPa and Poisson ratio was 0.3. The constitutive model defined in Equation (9) was also used.

(a)　　　　　　　　　　　　　　　　　　　(b)
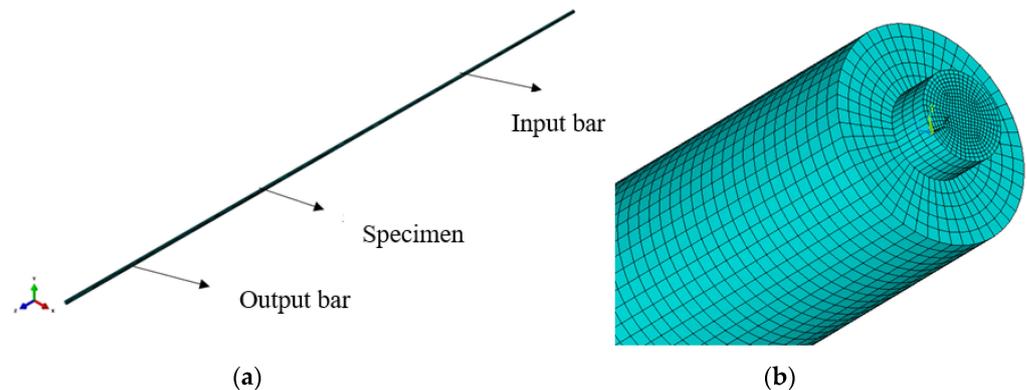
Figure 16. FE model of SHPB test.

4.5. Comparison of the Numerical and Test Results

4.5.1. Low Temperature (0 °C)

It was complicated to include the low temperature and the strain rate effect. The constitutive model at 0 °C is discussed first. As listed in Table 2, the C and p values are taken as 2639.4, 5.40, separately. A series of numerical analyses was performed in test conditions at 0 °C. Figure 17a–d gives the comparison of the test and numerical results with a low strain rate. The yield stresses obtained by the numerical method are lower than the tests in the case of 0.01, 0.1, and 1 s^{-1}, whereas the ultimate tension stresses coincide well with the tests.

The results of the high strain rate are illustrated in Figure 17e,f. The errors between the stress–strain curves of the tests and the numerical analysis are large.

Comparing the numerical results with the tests, the average error is 6.8%. The numerical results of $C = 2639.4$, and $P = 5.40$ are set as the sample data to fit the new values of C and P. The iterative approximate process is illustrated in Figure 18, with the average errors. After three iterative steps, the average error was 4.8% as the $C = 1974.7$, $P = 2.4$.
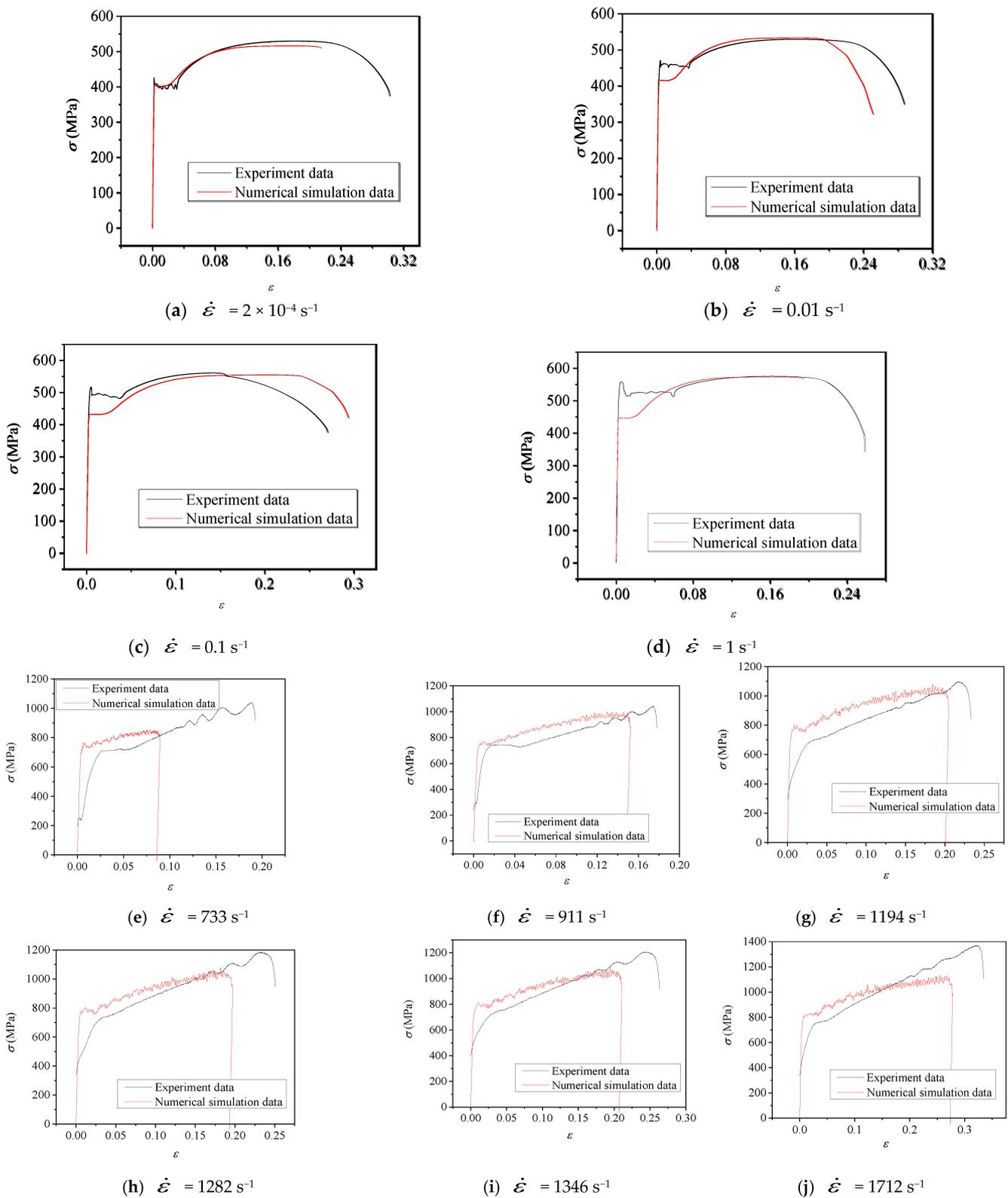
Figure 17. Comparison of the test and the numerical results of *C* = 2639.4, *P* = 5.40.
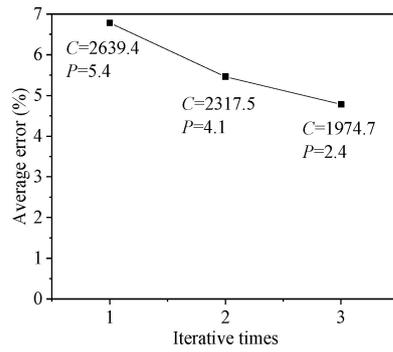
Figure 18. Average error with iterative times at 0 °C.

4.5.2. Other Temperatures

(1) Behaviour at Room Temperature (20 °C)

After four iterative calculations, the average error was 3.6%, thus less than 5%, with the constitutive coefficients C = 3599, P = 2.578. Figure 19 shows a comparison of the finite element results and experimental data at room temperature. It can be seen that the numerical results coincide with the experimental results, and the yield points are almost identical at low and high strain rates. It is shown that the constitutive model defined in Equation (9) can describe the strain rate effect of EH36 steel at room temperatures with strain rate effect accurately.
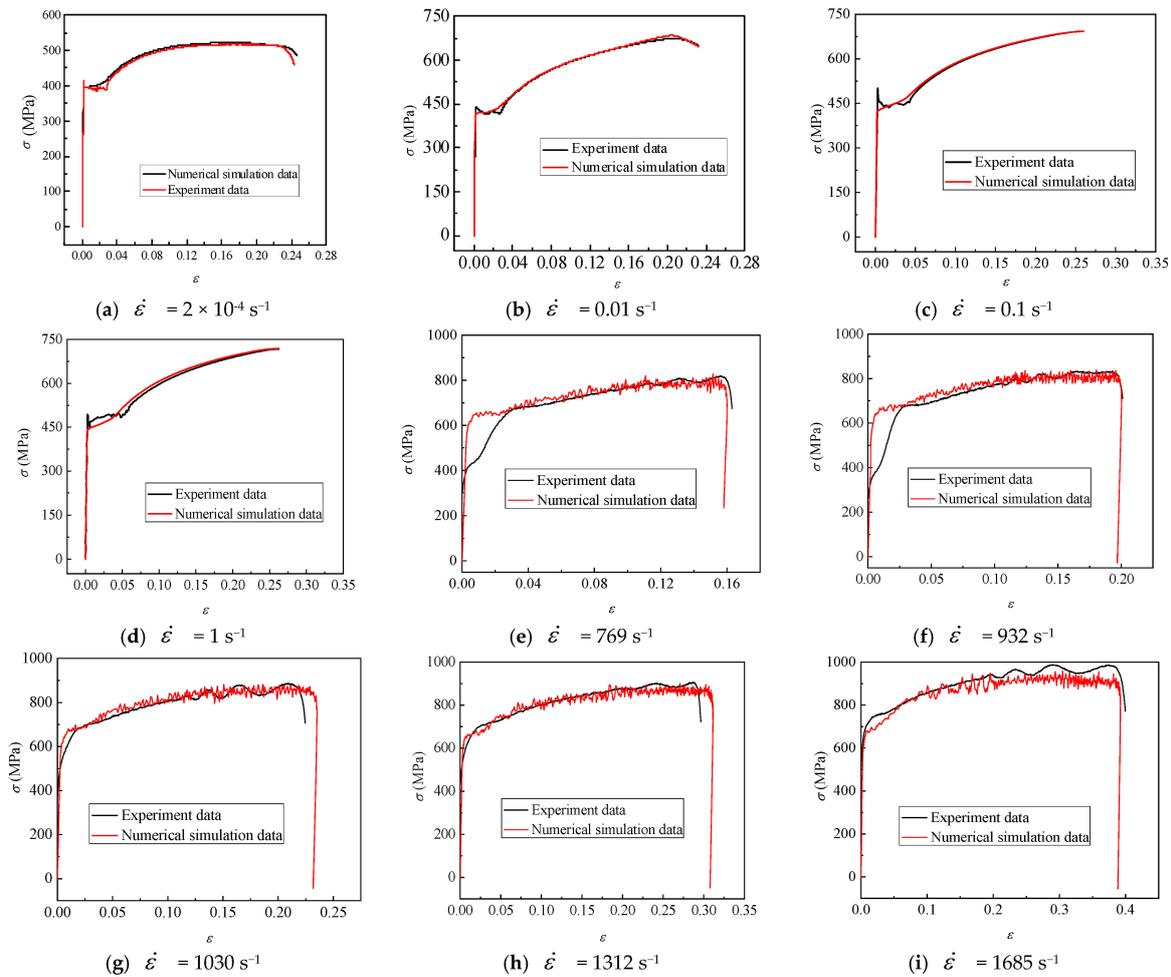
Figure 19. Comparison of numerical and test results at room temperature.

(2) Behaviour at $-20\ ^\circ$C

Using three iterative numerical analyses, the $C = 1982.6$ and $P = 3.2$ were obtained at $-20\ ^\circ$C, as the average error was 4.8%. The numerical results of the constitutive model with $C = 1982.6$ and $P = 3.2$ are compared with the experimental data with low and high strain rates in Figure 20.

(**a**) $\dot{\varepsilon} = 2 \times 10^{-4}\ \text{s}^{-1}$

(**b**) $\dot{\varepsilon} = 0.01\ \text{s}^{-1}$

(**c**) $\dot{\varepsilon} = 0.1\ \text{s}^{-1}$

(**d**) $\dot{\varepsilon} = 1\ \text{s}^{-1}$

(**e**) $\dot{\varepsilon} = 874\ \text{s}^{-1}$

(**f**) $\dot{\varepsilon} = 1031\ \text{s}^{-1}$

(**g**) $\dot{\varepsilon} = 1191\ \text{s}^{-1}$

(**h**) $\dot{\varepsilon} = 1380\ \text{s}^{-1}$

(**i**) $\dot{\varepsilon} = 1676\ \text{s}^{-1}$

(**j**) $\dot{\varepsilon} = 1895\ \text{s}^{-1}$
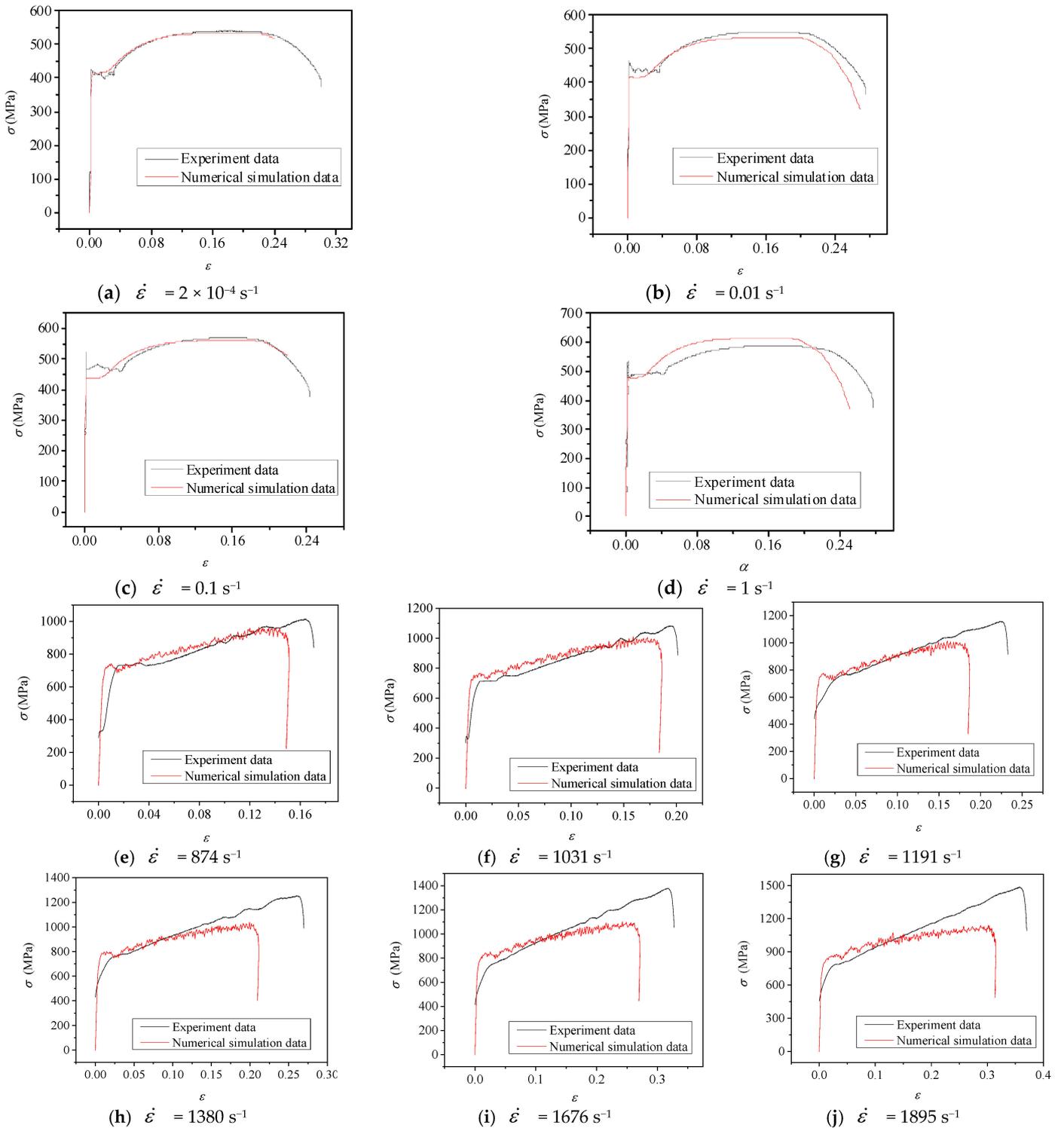
Figure 20. Comparison of numerical and test results at $-20\ ^\circ$C with high strain rate.

(3)　　Behaviour at −40 °C

The constitutive coefficients *C* = 2091.6 and *P* = 3.3 were obtained by three iterations at the low temperature of −40 °C, and the average error was 4.6%. The comparison of the numerical analysis and experiment data is shown in Figure 21 with low and high strain rates.

(a) $\dot{\varepsilon}$ = 2× 10⁻⁴ s⁻¹

(b) $\dot{\varepsilon}$ = 0.01 s⁻¹

(c) $\dot{\varepsilon}$ = 0.1 s⁻¹

(d) $\dot{\varepsilon}$ = 1 s⁻¹

(e) $\dot{\varepsilon}$ = 795 s⁻¹

(f) $\dot{\varepsilon}$ = 958 s⁻¹

(g) $\dot{\varepsilon}$ = 1098 s⁻¹

(h) $\dot{\varepsilon}$ = 1290 s⁻¹

(i) $\dot{\varepsilon}$ = 1535 s⁻¹

(j) $\dot{\varepsilon}$ = 1738 s⁻¹
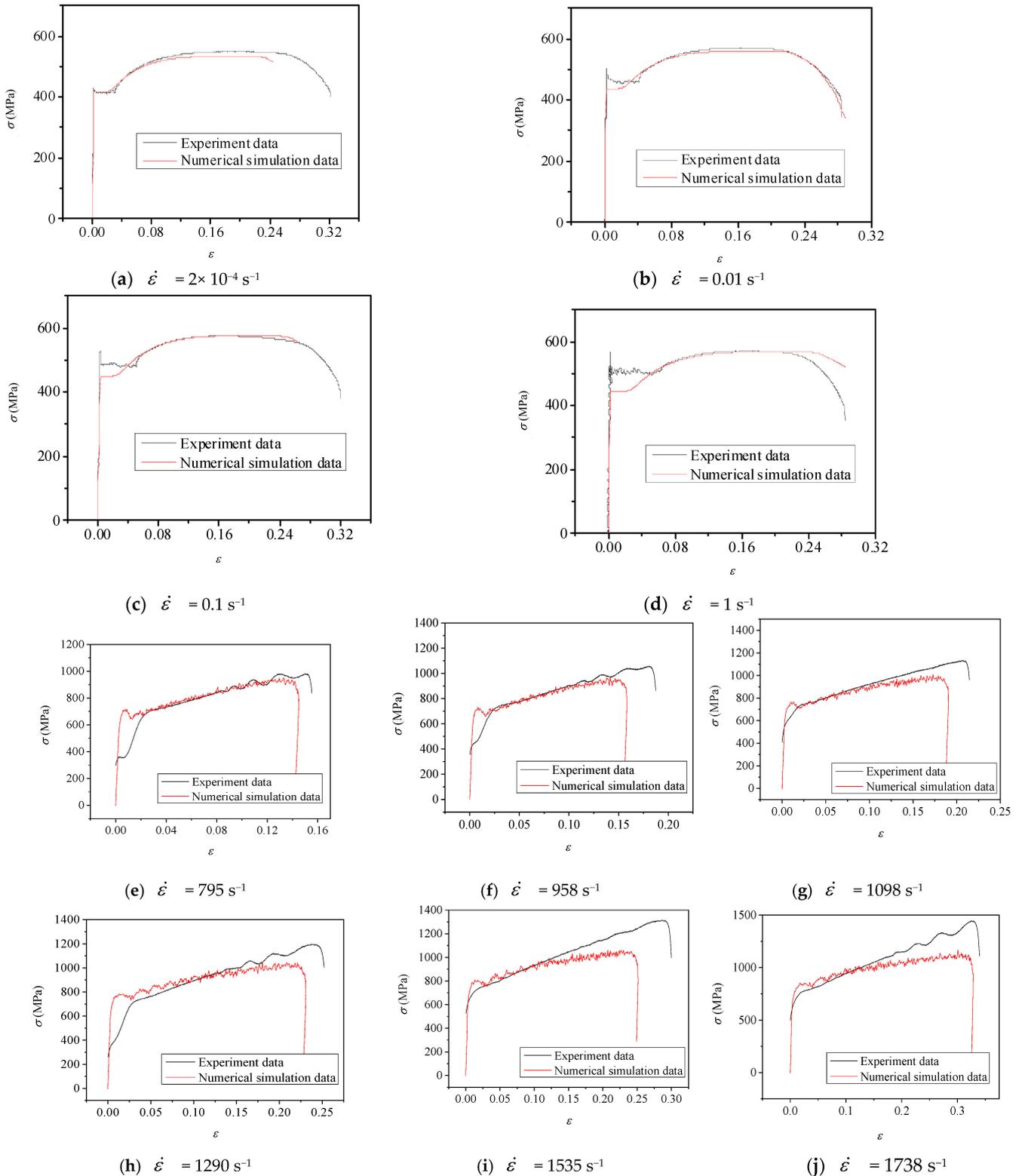
Figure 21. Comparison of numerical and test results at −40 °C.

(4)   Behaviour at −60 °C

Only low strain rate test results were used to fit the constitutive coefficients, $C = 225.42$ and $P = 3.95$, with an average error of 4.9%, thus less than 5%. Figure 22 shows the comparison of numerical and experiment data including low strain rate only.
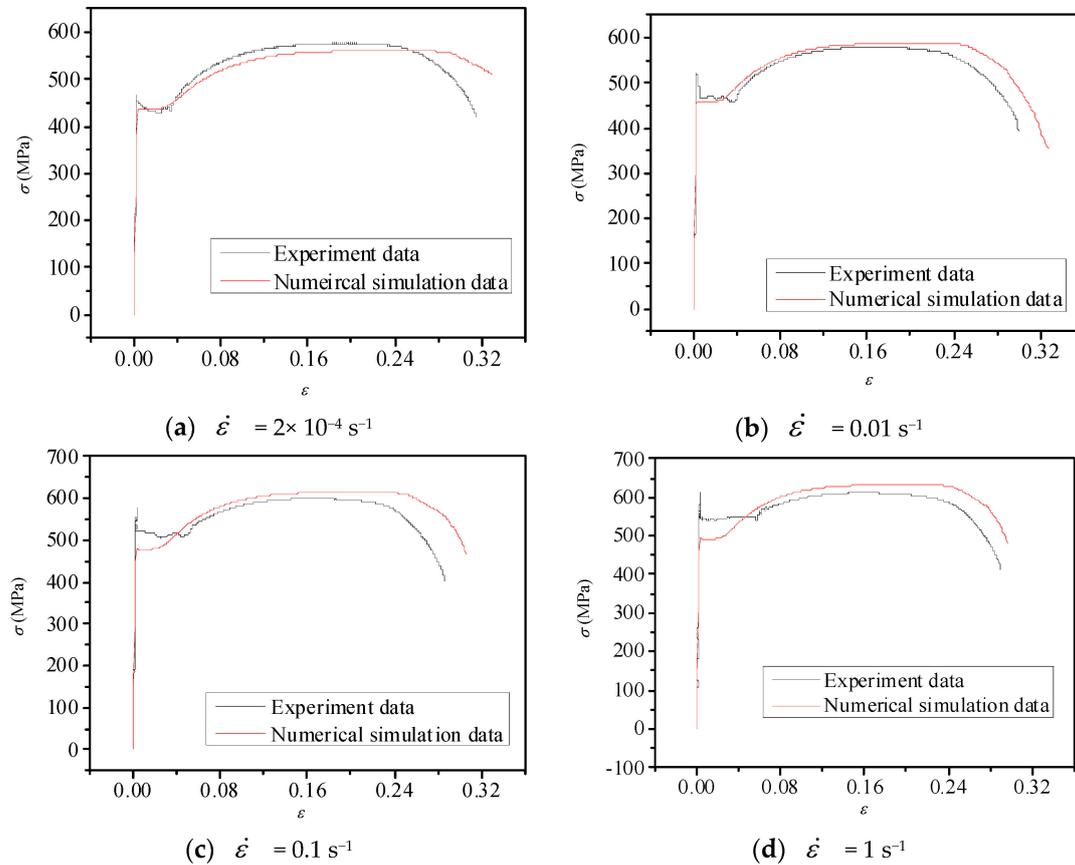
Figure 22. Comparison of numerical and test results at −60 °C.

From Figures 20–22, the stress–strain curves of the numerical results are compared with the experimental results at low temperatures −20 °C, −40 °C, and −60 °C. It can be seen that the numerical results show good agreement with the experiment considering the effect of low temperature and strain rate. Therefore, it can be concluded that the model of Equation (9) can be adopted as the stress–strain relationship of EH36 steel in the analysis of ship–ice interaction in the Arctic. However, it was found that the finite element results are conservative relative to the corresponding experimental results at a low strain rate.

5. Conclusions

In the present study, the mechanical behaviour of strain rate-sensitive steel EH36 under low-temperature test conditions were reported. The tests performed consisted of quasi-state and dynamic ones. First, the quasi-static tests ranging from room temperature to −60 °C were conducted. Then, the dynamic tests were performed on specimens at different strain rates under low temperatures. The tests of low strain rates of 0.01 s^{-1} to 1 s^{-1} were performed on an MTS testing machine and those of high strain rates of 700 s^{-1} to 2000 s^{-1} by SHPB. A constitutive model of EH36 was studied based on the Cowper-Symonds model, including the low temperature and strain rate effect. The results and conclusions can be summarized as follows:

(1) The experimental results indicate obvious strain rate effects on the nonlinear stress–strain behaviour at different strain rates of EH36 steel.

(2) EH36 steel has obvious temperature sensitivity. The yield stress of EH36 steel dramatically increased more than 10% nonlinearly with the decrease in temperature ranging from 20 °C to 60 °C, which indicated that low temperature can improve the yield stress, as well as the ultimate tensile stress. However, the toughness decreases with the temperature, shown as the decreasement of the fracture strain.

(3) An iterative approximated method was provided to fit the constants in the presented constitutive model. By performing a series of numerical analyses, a constitutive model for a certain low temperature was given by comparing the experimental and numerical results. It may describe the dynamic behaviour of EH36 at low temperatures accurately.

(4) An improved Cowper-Symonds model was established considering the effects of low temperature and strain rate by fitting the C, P constants in different temperatures ranging from 0 °C to 60 °C, which may describe the coupled effect of low temperature and strain rate.

Author Contributions: Conceptualization, J.Z., X.S. and C.G.S.; methodology, J.Z.; software, X.K.; validation, J.Z. and X.S.; formal analysis, X.K.; investigation, M.S.; resources, X.S.; data curation, J.Z.; writing—original draft preparation, J.Z.; writing—review and editing, C.G.S.; visualization, X.K.; supervision, C.G.S.; project administration, X.S. All authors have read and agreed to the published version of the manuscript.

Institutional Review Board Statement: Not applicable.

Informed Consent Statement: Not applicable.

Data Availability Statement: The data presented in this study are openly available at https://we.tl/t-hOcWbRIyb0 (accessed on 22 February 2023).

Conflicts of Interest: The authors declare no conflict of interest.

References

1. FMA. *Finnish-Swedish Ice Calss Rules*; Finnish Maritime Administration: Helsinki, Finland, 2002.
2. ABS. *Guidance Notes on Ice Class*; American Bureau of Shipping: Houston, TX, USA, 2005.
3. RMRS. *Rules for the Classification and Construction of Sea-Going Ships*; Russian Maritime Register of Shipping: Saint Petersburg, Russia, 2012.
4. He, X.; Guedes Soares, C. Pseudo-shakedown of rectangular plates under repeated impacts. *Mar. Struct.* **2022**, *85*, 103258. [CrossRef]
5. Liu, K.; Liu, B.; Villavicencio, R.; Wang, Z.; Guedes Soares, C. Assessment of material strain rate effects on square steel plates under lateral dynamic impact loads. *Ships Offshore Struct.* **2018**, *13*, 217–225. [CrossRef]
6. Ehlers, S.; Østby, E. Increased crashworthiness due to arctic conditions—The influence of sub-zero temperature. *Mar. Struct.* **2012**, *28*, 86–100. [CrossRef]
7. Paik, J.K.; Kim, K.J.; Lee, J.H.; Jung, B.G.; Kim, S.J. Test database of the mechanical properties of mild, high-tensile and stainless steel and aluminium alloy associated with cold temperatures and strain rates. *Ships Offshore Struct.* **2017**, *12* (Suppl. S1), S230–S256. [CrossRef]
8. Choung, J.; Nam, W.; Lee, J.-Y. Dynamic hardening behaviors of various marine structural steels considering dependencies on strain rate and temperature. *Mar. Struct.* **2013**, *32*, 49–67. [CrossRef]
9. DNV. *Rules for Classification for Ships Newbuildings*; Det Norske Veritas: Bærum, Norway, 2008.
10. IACS. *Requirements Concerning—POLAR CLASS*; International Association of Classification Societies: Hamburg, Germany, 2011.
11. Chen, W.W.; Song, B. *Split Hopkinson (Kolsky) Bar Design, Testing and Applications*; Springer: New York, NY, USA, 2011.
12. Dunand, M.; Mohr, D. Predicting the rate-dependent loading paths to fracture in advanced high strength steels using an extended mechanical threshold model. *Int. J. Impact Eng.* **2017**, *108*, 272–285. [CrossRef]
13. Liu, B.; Villavicencio, R.; Guedes Soares, C. On the failure criterion of aluminum and steel plates subjected to low-velocity impact by a spherical indenter. *Int. J. Mech. Sci.* **2014**, *80*, 1–15. [CrossRef]
14. Liu, B.; Guedes Soares, C. Effect of strain rate on dynamic responses of laterally impacted steel plates. *Int. J. Mech. Sci.* **2019**, *160*, 307–317. [CrossRef]
15. Forni, D.; Chiaia, B.; Cadoni, E. High strain rate response of S355 at high temperatures. *Mater. Des.* **2016**, *94*, 467–478. [CrossRef]

16. Mirmomeni, M.; Heidarpour, A.; Zhao, X.-L.; Hutchinson, C.R.; Packer, J.A.; Wu, C. Mechanical properties of partially damaged structural steel induced by high strain rate loading at elevated temperatures—An experimental investigation. *Int. J. Impact Eng.* **2015**, *76*, 178–188. [CrossRef]

17. Nemat-Nasser, S.; Guo, W.-G. Thermomechanical response of DH-36 structural steel over a wide range of strain rates and temperatures. *Mech. Mater.* **2003**, *35*, 1023–1047. [CrossRef]

18. Ibrahim, O.H.; Ibrahim, I.S.; Khalifa, T.A.F. Impact behavior of different stainless steel weldments at low temperatures. *Eng. Fail. Anal.* **2010**, *17*, 1069–1076. [CrossRef]

19. Getter, D.J.; Kantrales, G.C.; Consolazio, G.R.; Eudy, S.; Fallaha, S. Strain rate sensitive steel constitutive models for finite element analysis of vessel-structure impacts. *Mar. Struct.* **2015**, *44*, 171–202. [CrossRef]

20. Chen, J.; Li, J.; Li, Z. Experiment research on rate-dependent constitutive model of Q420 steel. *Constr. Build. Mater.* **2017**, *153*, 816–823. [CrossRef]

21. Su, J.; Guo, W.; Meng, W.; Wang, J. Plastic behavior and constitutive relations of DH-36 steel over a wide spectrum of strain rates and temperatures under tension. *Mech. Mater.* **2013**, *65*, 76–87. [CrossRef]

22. Detrois, M.; Antonov, S.; Tin, S.; Jablonski, P.D.; Hawk, J.A. Hot deformation behavior and flow stress modeling of a Ni-based superalloy. *Mater. Charact.* **2019**, *157*, 109915. [CrossRef]

23. Forni, D.; Chiaia, B.; Cadoni, E. Strain rate behaviour in tension of S355 steel: Base for progressive collapse analysis. *Eng. Struct.* **2016**, *119*, 164–173. [CrossRef]

24. Cowper, G.; Symonds, P. *Strain Hardening and Strain Rate Effects in the Loading of Cantilever Beams*; Brown University: Providence, RI, USA, 1957.

25. Shi, G.; Zhu, X.; Ban, H. Material properties and partial factors for resistance of high-strength steels in China. *J. Constr. Steel Res.* **2016**, *121*, 65–79. [CrossRef]

26. Bobbili, R.; Madhu, V.; Gogia, A.K. Neural network modeling to evaluate the dynamic flow stress of high strength armor steels under high strain rate compression. *Def. Technol.* **2014**, *10*, 334–342. [CrossRef]

27. Jones, N. *Structural Impact*; Cambridge University Press: Cambridge, MA, USA, 1997.

28. Jones, N. The credibility of predictions for structural designs subjected to large dynamic loadings causing inelastic behaviour. *Int. J. Impact Eng.* **2013**, *53*, 106–114. [CrossRef]

29. Hsu, S.S.; Jones, N. Quasi-static and dynamic axial crushing of thin-walled circular stainless steel, mild steel and aluminium alloy tubes. *Int. J. Crashworth.* **2004**, *9*, 195–217. [CrossRef]

30. *ASTM-E8*; Standard Test Methods for Tension Testing of Metallic Materials. American Society for Testing and Material: West Conshohocken, PA, USA, 2016.

31. Lin, Y.C.; Xia, Y.-C.; Chen, X.-M.; Chen, M.-S. Constitutive descriptions for hot compressed 2124-T851 aluminum alloy over a wide range of temperature and strain rate. *Comput. Mater. Sci.* **2010**, *50*, 227–233. [CrossRef]